Ceramics International 50 (2024) 6388–6394

Contents lists available at ScienceDirect

Ceramics International

journal homepage: www.elsevier.com/locate/ceramint

Effects of Bi_2O_3–CuO additives on microstructure and microwave properties of low-temperature-sintered NiCuZn ferrite ceramics

Tiantian Zeng [a,b], Lijun Jia [a,b,*], Zhihao Chen [a,b], Mingchao Yang [a,b], Rui Luo [a,b]

[a] State Key Laboratory of Electronic Thin Film and Integrated Devices, University of Electronic Science and Technology of China, Chengdu, 611731, China
[b] School of Electronic Science and Engineering, University of Electronic Science and Technology of China, Chengdu, 611731, China

ARTICLE INFO

Handling Editor: Dr P. Vincenzini

Keywords:
NiCuZn ferrite ceramics
Low-temperature sintering
Microstructure
Microwave properties

ABSTRACT

In this study, $(Ni_{0.2}Cu_{0.2}Zn_{0.6}O)_{1.03}(Fe_2O_3)_{0.97}$ ferrite ceramics with low microwave loss were synthesized through low-temperature sintering and doped with low eutectic mixture Bi_2O_3–CuO. Additionally, the influence of Bi_2O_3–CuO doping amount on phase composition, microstructure, and microwave performance of NiCuZn ferrite ceramics was systematically explored. It was found that all samples exhibited pure spinel phase. Moreover, scanning electron microscopy analysis revealed that appropriate doping amount of the Bi_2O_3–CuO mixture promoted grain growth and densification, leading to dense dual microstructure in NiCuZn ferrite ceramics. Notably, this microstructure significantly enhanced microwave properties of the material. For Bi_2O_3–CuO doping amount of 0.5 wt % and at sintering temperature of 910 °C, the NiCuZn ferrite ceramics exhibited low ferromagnetic resonance linewidth ($\Delta H \approx 90$ Oe), minimal dielectric loss ($\tan\delta_\varepsilon \approx 2.73 \times 10^{-4}$) at 9.3 GHz, and high saturation magnetization ($4\pi Ms \approx 3644$ Gauss). These results highlight the potential of Bi_2O_3–CuO as promising sintering aid, which could support the application of NiCuZn ferrite ceramics to microwave devices.

1. Introduction

With the rapid development of microwave and millimeter-wave integrated technologies, the demand for microwave ferrite devices in passive phased array systems has been steadily increasing. These devices require high-frequency operation, miniaturization, and integration, and low insertion loss characteristics are crucial for achieving a good performance [1]. To satisfy these requirements, microwave devices are expected to have low insertion loss characteristics. Notably, NiCuZn ferrite ceramics, which are critical materials for microwave ferrite devices, exhibit low microwave magnetic and dielectric losses, effectively reducing the insertion loss of microwave devices [2,3]. Additionally, the good saturation magnetization and dielectric constant of NiCuZn ferrites are beneficial for the miniaturization of electronic components [4,5].

Microwave magnetic loss, which is typically measured in terms of the ferromagnetic resonance linewidth (ΔH), is primarily determined by magnetocrystalline anisotropy broadening (ΔH_a) and pore-induced broadening (ΔH_p) in polycrystalline ferrite ceramics. NiCuZn ferrites possess a negative magnetic anisotropy constant (K_1). By introducing ions with positive K_1 (such as Co^{2+} ions), or adjusting the iron deficiency, the K_1 of NiCuZn ferrite ceramics can be effectively reduced, thereby decreasing ΔH_a [6–8]. For example, Sun et al. [8]. investigated the impact of iron deficiency on the microstructure and ΔH of NiCuZn ferrite ceramics and found that optimizing the degree of iron-deficiency resulted in improved density and reduced K_1, leading to a low ΔH (120 Oe) at a high sintering temperature of 1040 °C. Additionally, a detailed analysis revealed that ΔH_p exerted the most significant influence on ΔH, highlighting the significance of pore distribution in NiCuZn ferrite ceramics. Moreover, an appropriate degree of iron deficiency can hinder the formation of Fe^{2+} ions, contributing to reducing the dielectric loss in NiCuZn ferrite materials [9,10].

To achieve miniaturization and integration of microwave ferrite devices using low-temperature co-fired ceramic (LTCC) technology, it is common to incorporate low-melting-point oxides or glass into NiCuZn ferrite ceramics to reduce the sintering temperature to around 900 °C [11–16]. However, research on NiCuZn ferrite ceramics has been mainly limited to the radiofrequency (RF) range [17]. Therefore, it is of paramount importance to investigate the microwave properties of NiCuZn ferrite materials. Further reduction in the microwave losses and versatility in NiCuZn ferrite are crucial to enhancing the performance of electronic components and facilitating the processing of circuit systems. For instance, Liu et al. [18]. studied the impact of Bi_2O_3 doping on the

* Corresponding author. State Key Laboratory of Electronic Thin Film and Integrated Devices, University of Electronic Science and Technology of China, Chengdu, 611731, China.
E-mail address: jlj@uestc.edu.cn (L. Jia).

https://doi.org/10.1016/j.ceramint.2023.11.374
Received 4 October 2023; Received in revised form 15 November 2023; Accepted 28 November 2023
Available online 1 December 2023
0272-8842/© 2023 Elsevier Ltd and Techna Group S.r.l. All rights reserved.

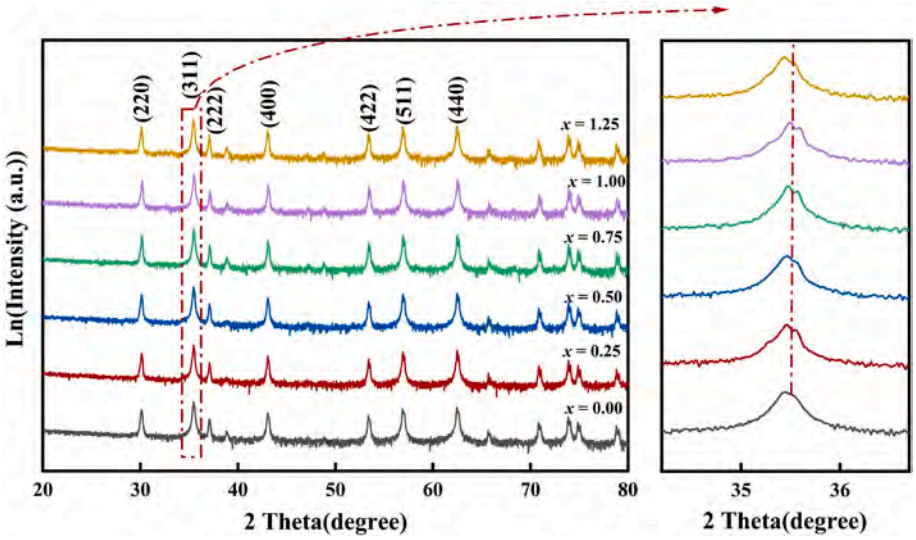

Fig. 1. XRD patterns of NiCuZn ferrite ceramics with different Bi_2O_3–CuO contents.

microwave performance of NiCuZn ferrite ceramics sintered at 900 °C and found that at a Bi_2O_3 doping amount of 3.0 wt %, the samples exhibited a ΔH of (200 Oe). Ji et al. [19]. discovered that doping with a certain amount of Bi_2O_3 promoted grain growth but also resulted in the formation of abnormal grains. Furthermore, Zheng et al. [20]. found that incorporating a suitable amount of low-melting-point Bi_2O_3–ZnO–B_2O_3 (BZB) glass in iron-deficient $(Ni_{0.2}Cu_{0.2}Zn_{0.6}O)_{1.03}(Fe_2O_3)_{0.97}$ promoted grain growth and densification, leading to the formation of NiCuZn ferrite ceramics with a uniform and dense microstructure consisting of fine grains. However, under low-temperature sintering conditions, the ferromagnetic resonance linewidth of NiCuZn ferrite remained high (150 Oe), and its dielectric properties were not studied.

In a previous study, we discovered that incorporating a low eutectic mixture can effectively control the grain and pore size distribution in ferrite ceramics [21–25]. Bi_2O_3 and CuO are good sintering aids, which have different melting points. During the sintering process, the Bi_2O_3–CuO mixture first forms a eutectic compound and then melts to form a liquid phase, facilitating the movement and arrangement of grains in the sintering process, which results in a dense dual microstructure. This is expected to significantly reduce ΔH_p in ferrite materials [21]. To achieve a low ΔH, low dielectric loss, and high saturation magnetization ($4\pi Ms$), in this study, $(Ni_{0.2}Cu_{0.2}Zn_{0.6}O)_{1.03}(Fe_2O_3)_{0.97}$ was selected as the primary composition, and the low eutectic mixture Bi_2O_3–CuO was selected as the sintering aid. We investigated the influence of the amount of added Bi_2O_3–CuO on the phase composition, microstructure evolution, densification process, and microwave properties of NiCuZn ferrite ceramics.

2. Experimental

2.1. Sample preparation

Composite microwave ferrite samples, here denoted as $(Ni_{0.2}Cu_{0.2}Zn_{0.6}O)_{1.03}(Fe_2O_3)_{0.97}$ with x wt % Bi_2O_3–CuO mixture (x = 0.00, 0.25, 0.50, 0.75, 1.00, 1.25), were prepared. First, the raw materials were weighed according to the chemical formula; the purity of all raw materials was greater than 99 %. Next, the powder was mixed with a suitable amount of deionized water and subjected to one round of ball milling in a planetary ball mill. The resulting slurry was dried and pre–fired at 875 °C for 2 h. Then, a fixed mass ratio of Bi_2O_3 and CuO (0.21:0.29) was added to the pre–fired powder, which was then subjected to a secondary ball milling step and drying. Approximately 10 wt % of polyvinyl alcohol binder was added to the dried powder for granulation, and the mixture was pressed into toroidal samples with dimensions of φ18 mm × φ 8mm × h 3 mm. Finally, the samples were sintered at 910 °C for 2 h.

2.2. Testing and characterization

Phase composition of all samples was analyzed via X-ray diffraction (XRD, DX-2700). The cross-sectional microstructure was observed via scanning electron microscopy (SEM, JOEL JSM-6490LV). The shrinkage of the sample was calculated by measuring the sample diameter before and after sintering for different sintering times. The shrinkage of the sample was then calculated as follows:

$$\text{shrinkage} = \ln((L_0 - L_1)/L_0) \tag{1}$$

where L_0 is the diameter of the sample before sintering, and L_1 is the diameter of the sample after sintering. The density of the samples was measured using the Archimedes drainage method with kerosene as the medium. The density was calculated as follows:

$$\rho = \frac{m_1 \times \rho_0}{m_2 - m_3} \tag{2}$$

where ρ_0 represents the density of kerosene, m_1 is the mass of the sample in air, m_2 is the mass of the sample after being fully immersed in the liquid and after removing the air trapped in its interior, and m_3 is the mass of the sample immersed in the liquid. Moreover, the porosity (P) of the samples was calculated based on the theoretical density and actual density using the following expression:

$$P = \left(1 - \frac{\rho}{d_x}\right) \times 100\% \tag{3}$$

where d_x is the theoretical density of spinel ferrite, obtained from XRD analysis. The Curie temperature (Tc) of the samples was determined using thermogravimetric analysis. The magnetic hysteresis loop and saturation magnetization were measured using a vibrating sample magnetometer (VSM-220). The ferromagnetic resonance linewidth of the samples was evaluated using the perturbation method in a TE106 resonant cavity at 9.3 GHz. The microwave dielectric properties of the ferrite materials were characterized in the X-band following the IEC standard.

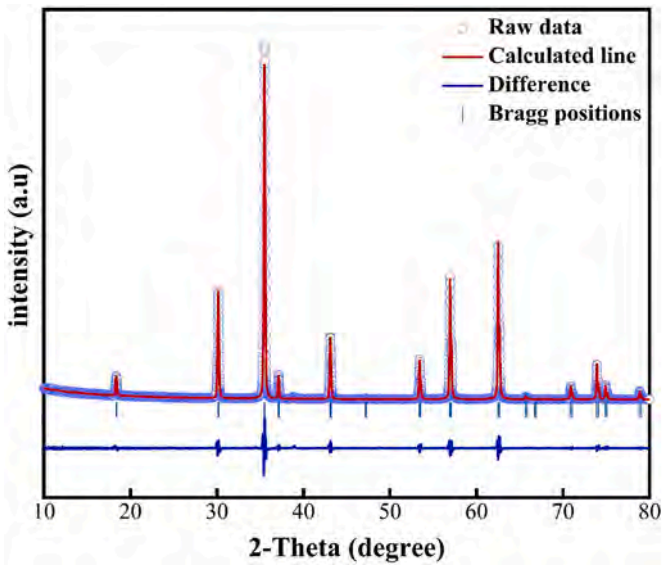

Fig. 2. Rietveld refinement of undoped NiCuZn ferrite ceramics ($x = 0.00$).

Table 1
Refined structural of NiCuZn ferrite ceramics with different Bi_2O_3–CuO contents.

	$x = 0.00$	$x = 0.25$	$x = 0.50$	$x = 0.75$	$x = 1.00$	$x = 1.25$
a (Å)	8.4153	8.4167	8.4171	8.4175	8.4182	8.4197
R_{wp}	12.11	13.19	12.54	13.97	12.90	13.53
R_p	9.74	9.62	9.95	10.15	10.13	10.62
χ^2	1.89	1.59	1.20	2.21	1.23	2.28
V (Å^3)	595.96	596.25	596.33	596.43	596.56	596.89

3. Results and discussion

3.1. Analysis of phase, microstructure, and sintering behavior

Fig. 1 presents the XRD patterns of NiCuZn ferrite samples sintered at 910 °C with different amounts of the low eutectic mixture Bi_2O_3–CuO. To better understand whether other phases are formed in NiCuZn ferrite due to the presence of the Bi_2O_3–CuO mixture, the intensity of the XRD peaks was represented in logarithmic form. The patterns reveal characteristic peaks of the spinel phase, namely (220), (311), (222), (400), (422), (511), and (440) peaks, without any additional diffraction peaks. It is worth noting that the (311) diffraction peak, shown in the inset of Fig. 1, shifts slightly toward smaller angles with increasing Bi_2O_3–CuO doping amount. This shift can be attributed to the lattice expansion resulting from the partial substitution of Fe^{3+} ions ($r = 0.67$ Å) in the ferrite lattice structure with larger-radius Bi^{3+} ions ($r = 1.08$ Å) and Cu^{2+} ions ($r = 0.72$ Å) [26].

Further analysis of the XRD data was conducted using GSAS-II software, and the refinement results are presented in Fig. 2. All diffraction peaks of the samples match well those of the standard PDF card (JCPDS #48–0489), indicating that all samples consist of a single spinel phase. The detailed refinement results are listed in Table 1, showing low values of R_{wp}, R_p, and χ^2, which confirms the reliability of the refinement results [27]. With an increase in Bi_2O_3–CuO doping amount, the lattice constant of the spinel ferrite gradually increases. The increased lattice volume activates lattice particles, facilitating the occurrence of solid-phase reactions in the NiCuZn ferrite ceramics.

Fig. 3 displays SEM images of NiCuZn ferrite samples doped with different Bi_2O_3–CuO doping amounts. In Fig. 3(a), the sample without any sintering aid exhibits a loose and porous fine-grain structure. As the amount of Bi_2O_3–CuO mixture increases, the ferrite grains gradually become larger. Notably, a dense and uniform microstructure (large grain size ~3 μm; small grain size ~1.3 μm) was clearly visible in the samples, as shown in Fig. 3(c). This dual microstructure significantly improves the densification of the ferrite materials [25,28]. However, a substantial increase in the amount of Bi_2O_3–CuO mixture results in significant grain growth, as indicated in Fig. 3(d)–(f), with some grain sizes exceeding 50 μm. Additionally, these enlarged grains contain numerous pores, resulting in the deterioration of the densification of the samples. This can be attributed to the fact that upon increasing the amount of the Bi_2O_3–CuO mixture, the sintering process is mainly governed by the liquid-phase sintering mechanism. This, combined with capillary force and lattice distortion of the ferrite, leads to the formation of abnormal

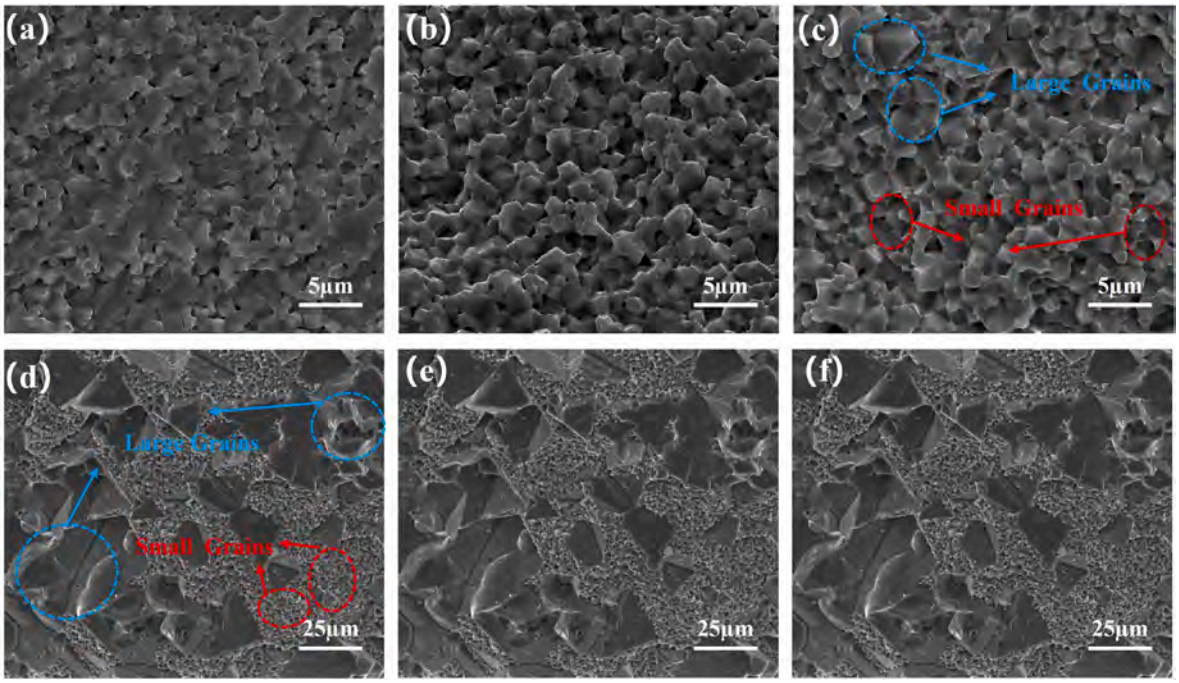

Fig. 3. SEM images of NiCuZn ferrite ceramics with different Bi_2O_3–CuO amounts. (a) $x = 0.00$, (b) $x = 0.25$, (c) $x = 0.50$, (d) $x = 0.75$, (e) $x = 1.00$, (f) $x = 1.25$.

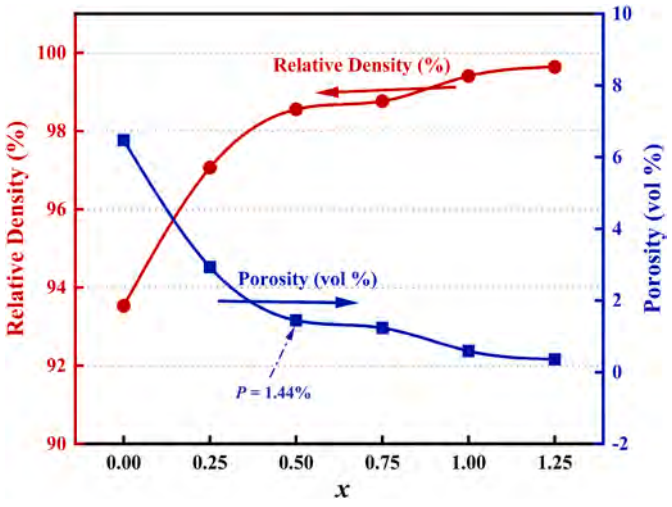

Fig. 4. Relative densities and porosities of NiCuZn ferrite ceramics with different Bi_2O_3–CuO contents.

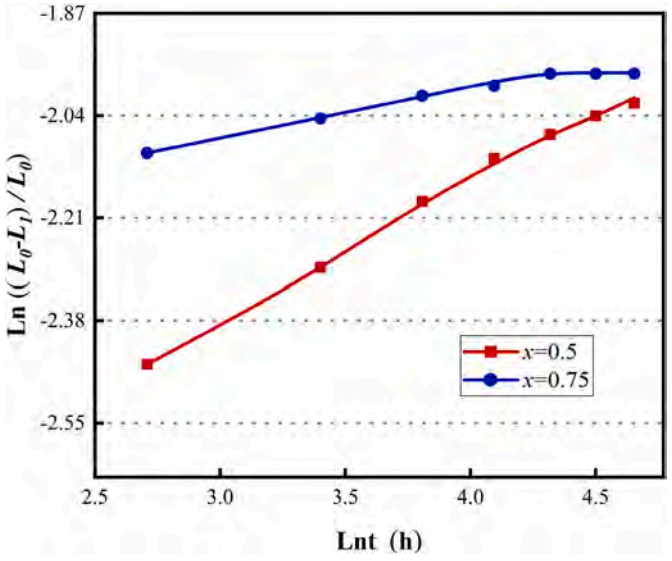

Fig. 5. Relationship between shrinkage rate and heating time for NiCuZn ferrite ceramics with different Bi_2O_3–CuO contents.

grains [29,30]. Fig. 4 shows that as the doping amount of Bi_2O_3–CuO mixture increases, the relative density of the samples also increases, reaching a relatively high value, while the porosity follows the opposite trend. When the doping amount of Bi_2O_3–CuO is $x = 0.50$, the porosity of the samples is significantly reduced, which is consistent with the results of the microstructure changes depicted in Fig. 3.

The crystallization kinetics of samples with different Bi_2O_3–CuO contents under isothermal conditions are compared in Fig. 5. At $x =$ 0.50 wt %, the logarithm of the shrinkage shows a linear relationship with the logarithm of the heating time, indicating that the sintering process is primarily governed by solid-state sintering mechanisms [31]. By contrast, at $x = 0.75$ wt %, a significant inflection point appears in the shrinkage rate curve. This can be attributed to the joint influence of capillary forces generated by low-melting-point liquid phases at grain boundaries and the lattice distortion of the ferrite, which promotes material transport and grain growth processes, leading to abnormal grain growth phenomena.

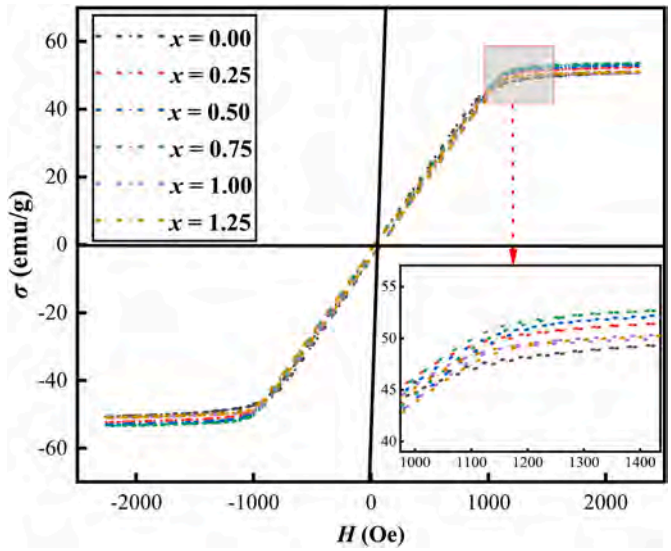

Fig. 6. Magnetic hysteresis loops of NiCuZn ferrite ceramics with different Bi_2O_3–CuO contents.

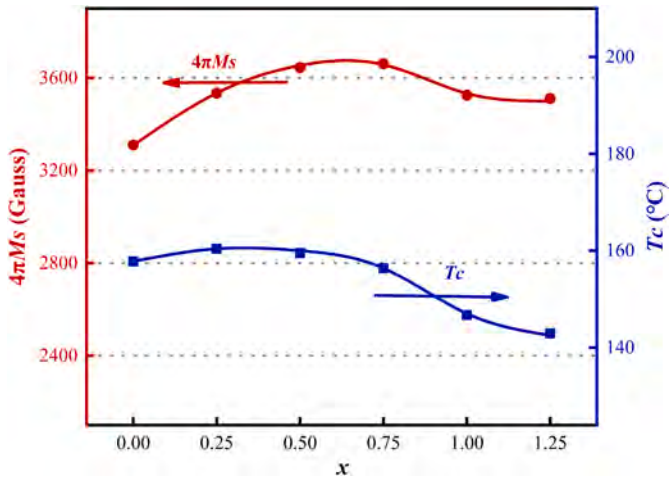

Fig. 7. Saturation magnetization ($4\pi Ms$) and Curie temperature (Tc) of NiCuZn ferrite ceramics with different Bi_2O_3–CuO contents.

3.2. Analysis of magnetic properties

The magnetic hysteresis loops of the NiCuZn ferrite ceramic samples with various Bi_2O_3–CuO doping amounts are shown in Fig. 6. As the magnetic field strength approaches ~1200 Oe, the magnetization of the sample aligns with the external magnetic field direction, approaching saturation. The hysteresis loops exhibit soft magnetic characteristics typical of ferrite samples. From Fig. 6, it is evident that the saturation magnetization (Ms) initially increases and then declines with increasing doping amount of the Bi_2O_3–CuO mixture. At $x = 0.75$ wt %, the Ms reaches its peak value. This phenomenon can be attributed to the enhanced completion of solid-state reactions facilitated by the Bi_2O_3–CuO sintering aid, which effectively promotes the densification process and grain growth, leading to an increase in Ms of the samples [17].

Fig. 7 illustrates the variations in saturation magnetization ($4\pi Ms$) and Curie temperature (Tc) of the NiCuZn ferrite ceramic samples. The $4\pi Ms$ value of spinel ferrites is primarily affected by sample density, grain size, and the superexchange interaction between tetrahedral (A-site) and octahedral (B-site) ions [32,33]. At lower Bi_2O_3–CuO contents, the mixture enhances sample densification, resulting in an increase in the $4\pi Ms$ value with increasing density. As the doping amount of

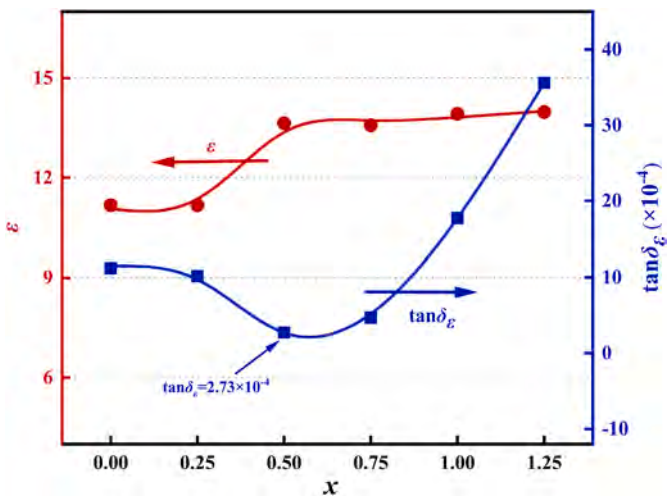

Fig. 8. Dielectric constant ε_r and dielectric loss $\tan\delta_\varepsilon$ of NiCuZn ferrite ceramics with different Bi_2O_3–CuO contents.

Bi_2O_3–CuO increases, result in a continuous decrease in the porosity of ferrites, as well as a gradual increase in grain size. leading to an increase in the $4\pi Ms$ value. At $x = 0.75$ wt %, $4\pi Ms$ reaches its peak value (~3700 Gauss). With the further addition of the Bi_2O_3–CuO, which substitutes some Fe^{3+} ions at B-sites with non-magnetic Bi^{3+} ions and weakly magnetic Cu^{2+} ions, reduce the total magnetic moment (M_B) of the B-sites of the ferrites. This weakens the superexchange interaction between A- and B-sites and leads to a decrease in $4\pi Ms$. In addition, being an intrinsic parameter, the Curie temperature (Tc) is mainly influenced by material properties [34]. At low doping amounts, an appropriate amount of the sintering aid promotes the completion of solid-state reactions, resulting in a slight increase in Tc. However, with further increases in the Bi_2O_3–CuO content, the substitution of B-site Fe^{3+} ions weaken the superexchange interaction, leading to a reduction in Tc.

Fig. 8 presents the impact of Bi_2O_3–CuO mixture doping on the dielectric properties of the NiCuZn ferrite samples. At microwave frequencies, the dielectric constant (ε_r) of spinel ferrites is usually around 13, and it is mainly determined by material density. The dielectric loss variation is primarily associated with the concentration of Fe^{2+} ions and porosity [1,19]. From Fig. 8, it can be seen that with increasing Bi_2O_3–CuO content, the dielectric constant of the samples first increases slowly from around 11 to around 14, and then it remains constant at stays around 14 as the doping amount of the Bi_2O_3–CuO mixture increases further. Additionally, due to high-temperature oxygen deficiency during sintering, the following chemical reaction occurs within the ferrite:

$$Fe^{2+} \Leftrightarrow Fe^{3+} + e. \quad (4)$$

This reaction enhances electron conduction and reduces the resistivity of the ferrite, resulting in increased dielectric loss [35]. In summary, the addition of an appropriate amount of Bi_2O_3–CuO effectively improves both the completion of solid-state reactions and density, leading to a reduced dielectric loss. At $x = 0.50$ wt %, the samples exhibit the lowest dielectric loss tangent ($\tan\delta_\varepsilon = 2.73 \times 10^{-4}$). However, further addition of sintering aids may result in the concentration of Fe^{2+} ions becoming the primary factor affecting the dielectric loss value.

To investigate the influence of Bi_2O_3–CuO mixture doping on the concentration of Fe^{2+} ions, the Fe_{2p} energy spectrum of the NiCuZn ferrite samples was analyzed by means of X-ray photoelectron spectroscopy (XPS). The binding energies of Fe^{2+} in the $2p_{1/2}$ and $2p_{3/2}$ peak regions are known to be 724.2 and 710.5 eV, respectively, while those of Fe^{3+} in the $2p_{1/2}$ and $2p_{3/2}$ peak regions are 726.8 and 712.5 eV, respectively [36]. The analysis in Fig. 9 indicates that as the Bi_2O_3–CuO doping amount increases, a gradual increase in the area ratio of the Fe^{2+} to Fe^{3+} peaks, with corresponding values of 0.6817, 0.7267, 0.7394, 0.7976, 0.8111, and 1.2965, respectively. During high-temperature sintering, some Cu^{2+} ions substitute Fe^{3+} ions at the B-sites of ferrites,

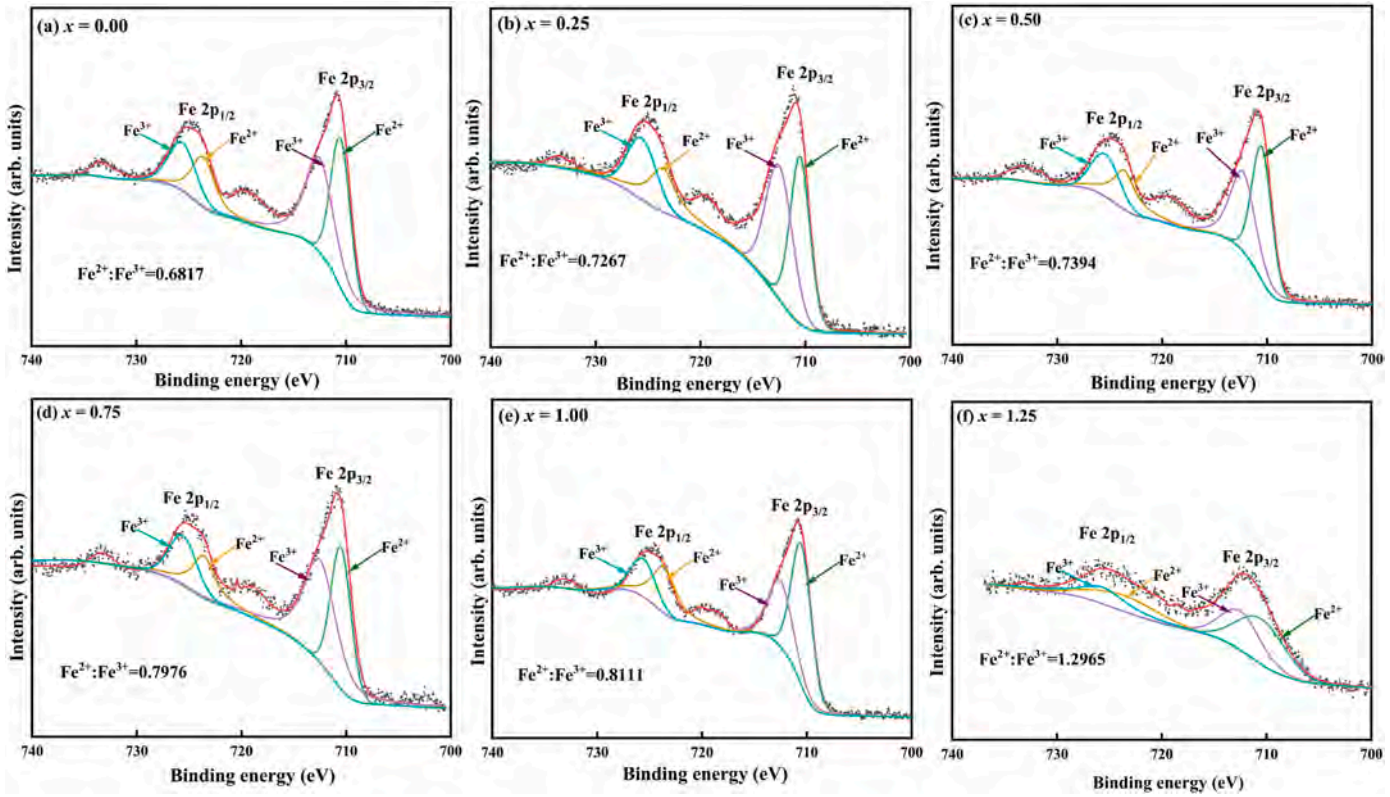

Fig. 9. Fe $_{2p}$ XPS spectra of NiCuZn ferrite ceramics with different Bi_2O_3–CuO contents.

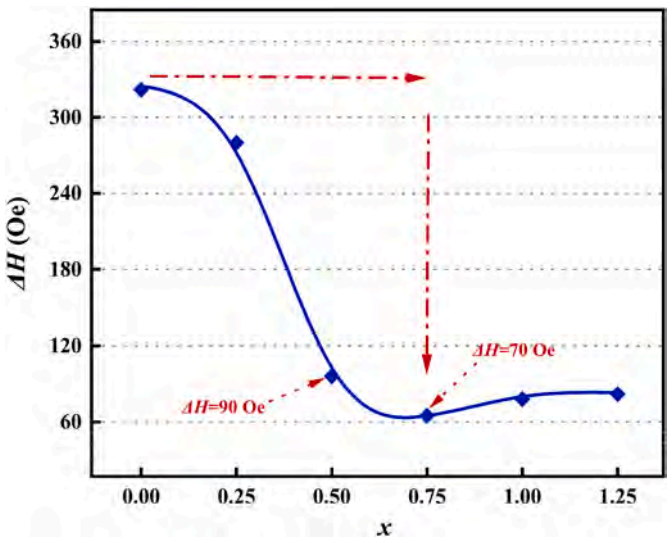

Fig. 10. Ferromagnetic resonance line width (Δ*H*) of NiCuZn ferrite ceramics with different Bi_2O_3–CuO contents.

resulting in a minor increase in the concentration of Fe^{2+} ions [37]. In summary, NiCuZn ferrite ceramics doped with an appropriate amount of Bi_2O_3–CuO are expected to have low dielectric loss values due to their high density and low Fe^{2+} concentration degrees.

The magnetic loss in polycrystalline ferrites is characterized by ΔH, which can be expressed as [38].

$$\Delta H = \Delta H_a + \Delta H_p + \Delta H_i = 2.07\left(\frac{H_a}{4\pi M_S}\right) + 1.5(4\pi M_S)P + \Delta H_i \quad (4)$$

where, ΔH_a, ΔH_p, ΔH_i, and P denote magneto-crystalline anisotropy, porosity-induced linewidth broadening, intrinsic linewidth, and porosity of grains, respectively. Given that ΔH_i is typically significantly smaller than the other factors contributing to linewidth broadening, we primarily focus on analyzing the contributions of ΔH_a and ΔH_p [39]. Fig. 10 presents the variation in microwave magnetic loss (ΔH) of NiCuZn composite ferrite samples with different Bi_2O_3–CuO contents. With increasing Bi_2O_3–CuO doping amount, ΔH initially experiences a rapid decrease, and then increases gradually.

Without the addition of sintering aids, the sample is characterized by a small grain size and many pores at grain boundaries, leading to reduced density and an increase in ΔH_p. With an increase in the doping amount of Bi_2O_3–CuO mixture, the pore content in the sample decreases, and the saturation magnetization increases, leading to a decrease in both ΔH_p and ΔH_a. At $x = 0.75$ wt %, the samples exhibit the lowest ΔH (~70 Oe). In conclusion, an appropriate doping amount of the Bi_2O_3–CuO mixture effectively improves both the completion of solid-state reactions and density, resulting in an excellent ΔH of NiCuZn ferrite ceramics during low-temperature sintering processes.

4. Conclusions

This study highlights the positive effect of incorporating the low eutectic mixture Bi_2O_3–CuO for optimizing the microstructure and enhancing the magnetic properties of NiCuZn ferrite ceramics. Through careful tuning of the Bi_2O_3–CuO ratio and doping amount, the solid-phase reaction and densification process are facilitated, resulting in NiCuZn ferrite ceramics with exceptional magnetic properties and low microwave loss at a low sintering temperature. Specifically, when the Bi_2O_3–CuO doping amount was 0.50 wt % and the sintering temperature was 910 °C, the NiCuZn ferrite ceramics exhibited remarkable magnetic characteristics, including high $4\pi Ms$ (~3644 Gauss), low ΔH (~90 Oe), and minimum dielectric loss ($\tan\delta_\varepsilon \approx 2.73 \times 10^{-4}$). Therefore, the low eutectic mixture Bi_2O_3–CuO emerges as a promising sintering additive for enhancing the magneto-electric properties of NiCuZn ferrite materials, facilitating their application to microwave ferrite devices.

Declaration of competing interest

The authors declare that they have no known competing financial interests or personal relationships that could have appeared to influence the work reported in this paper.

Acknowledgments

This work was supported by the National Key Scientific Instrument and Equipment Development Project under Grant No.51827802. National Natural Science Foundation of China under Grant No. 51572041.

References

[1] Q. Zhang, X.L. Tang, F.Y. Huang, X.H. Wu, Y.X. Li, H. Su, Enhanced microwave dielectric properties of wolframite structured $Zn_{1-x}Cu_xWO_4$ ceramics with low sintering temperature, J. Materiomics 7 (2021) 1309–1317.
[2] T. Wang, G.H. Dong, Y.X. Ma, H.X. Liu, Z.Y. Zhou, M. Liu, Stress-induced controllable magnetic properties in flexible epitaxial $Mn_{0.5}Zn_{0.5}Fe_2O_4$ ferrite films, J. Materiomics 8 (2022) 596–600.
[3] J.L. Pan, R.J. Zhang, J. Ling, M. Wang, Z.C. Li, Z. Zhen, L.M. He, H.W. Zhu, Controllable preparation and microwave absorption properties of shape anisotropic Fe_3O_4 nanobelts, J. Materiomics 7 (2021) 957–966.
[4] S.A. Oliver, P.M. Zavracky, N.E. McGruer, R. Schmidt, A monolithic single-crystal yttrium iron garnet/silicon X-band circulator, IEEE Microw. Guid. Wave Lett. 7 (1997) 239–241.
[5] Y. Yang, J. Li, H.W. Zhang, G. Wang, Y.H. Rao, G.W. Gan, TiO_2 tailored low loss NiCuZn ferrite ceramics having equivalent permeability and permittivity for miniaturized antenna, J. Magn. Magn Mater. (2019) 487.
[6] K.W. Li, K. Sun, C. Chen, X. Liu, R.D. Guo, H. Liu, Z. Yu, X.N. Jiang, Z.W. Lan, Tunable ferromagnetic resonance linewidth of cobalt-substituted NiCuZn ferrites, J. Alloys Compd. 752 (2018) 395–401.
[7] Y. Yang, J. Li, H.W. Zhang, J. Li, F. Xu, G. Wang, F. Gao, H.K. Su, Nb^{5+} ion substitution assisted the magnetic and gyromagnetic properties of NiCuZn ferrite for high frequency LTCC devices, Ceram. Int. 48 (2022) 12490–12496.
[8] K. Sun, Z.Y. Pu, Y. Yang, L.L. Chen, Z. Yu, C.J. Wu, X.N. Jiang, Z.W. Lan, Rietveld refinement, microstructure and ferromagnetic resonance linewidth of iron-deficiency NiCuZn ferrites, J. Alloys Compd. 681 (2016) 139–145.
[9] L. Guo, J. Li, Y. Yang, G. Wang, Y.H. Rao, G.W. Gan, H.W. Zhang, Bi_2O_3-doping controlled magnetic and dielectric properties of low-temperature co-fired NiCuZn ferrite for high-frequency applications, J. Mater. Sci. Mater. Electron. 30 (2019) 15437–15443.
[10] Y.Y. Huang, L.Y. Zhang, R.Y. Jing, Y. Yang, V. Shur, X.Y. Wei, L. Jin, Superior piezoelectric performance with high operating temperature in bismuth ferrite-based multiferroics, J. Mater. Sci. Technol., 169 (2024) 172-181..
[11] M. Zhang, V. Koval, Y. Shi, Y.J. Yue, C.L. Jia, J.G. Wu, G. Viola, H.X. Yan, Magnetoelectric coupling at microwave frequencies observed in bismuth ferrite-based multiferroics at room temperature, J. Mater. Sci. Technol. 137 (2023) 100–103.
[12] C. Chen, S. Qian, Q. Zhang, X.M. Zhang, T.H. Yao, Structural evolution and magnetic properties of NiCuZn ferrite synthesized via combustion reaction method, Inorg. Chem. Commun. 147 (2023).
[13] X.Y. Wang, H.W. Zhang, L. Shi, J. Li, L.C. Jin, L. Cheng, L.J. Jia, D.A. Zhang, Y. L. Liao, Synthesis and magnetic properties of low-temperature sintered, LMZBS glass-doped dense NiCuZn ferrites, Ceram. Int. 48 (2022) 19011–19016.
[14] R. Peng, Q. Zhao, Y.X. Li, J. Li, H.W. Zhang, Magnetic and dielectric properties of low-temperature sintered NiCuZn/$CaTiO_3$ composite dual-performance materials, J. Alloys Compd. (2022) 910.
[15] S.Q. Yan, S. Liu, L.H. He, J. He, S.X. Huang, L.W. Deng, Investigation on microstructure and magnetic properties in V_2O_5 doped NiCuZn ferrite, Mater. Res. Express 6 (2019).
[16] Q. Zhang, H. Su, H.W. Zhang, X.L. Tang, Bond, vibration and microwave dielectric characteristics of $Zn_{1-x}(Li_{0.5}Bi_{0.5})_xWO_4$ ceramics with low temperature sintering, J. Materiomics 8 (2022) 392–400.
[17] Y. Yang, J. Li, H.W. Zhang, L.C. Jin, F. Xu, G.W. Gan, G. Wang, D.D. Wen, Enhanced gyromagnetic properties of NiCuZn ferrite ceramics for LTCC applications by adjusting MnO_2-Bi_2O_3 substitution, Ceram. Int. 44 (2018) 19370–19376.
[18] Y.L. Liu, Y.X. Li, H.W. Zhang, Q.H. Yang, Study on microwave properties of low temperature fired NiZnCu gyromagnetic ferrite, J. Appl. Phys. 105 (2009).
[19] X.R. Ji, C. Shen, Y. Zhao, H. Zheng, Q. Wu, Q.Y. Zhang, L. Zheng, P. Zheng, Y. Zhang, Enhanced electromagnetic properties of low-temperature sintered NiCuZn ferrites by doping with Bi_2O_3, Ceram. Int. 48 (2022) 20315–20323.
[20] Y.H. Zheng, L.J. Jia, F. Xu, G. Wang, X.L. Shi, H.W. Zhang, Microstructures and magnetic properties of low temparature sintering NiCuZn ferrite ceramics for microwave applications, Ceram. Int. 45 (2019) 22163–22168.

[21] F. Xie, L.J. Jia, Y.P. Zhao, J. Li, T.C. Zhou, Y.L. Liao, H.W. Zhang, Low-temperature sintering and ferrimagnetic properties of LiZnTiMn ferrites with Bi_2O_3-CuO eutectic mixture, J. Alloys Compd. 695 (2017) 3233–3238.
[22] Y. Zhang, X.L. Tang, X.H. Wu, J.B. Chen, Y.L. Jing, H. Su, Effect of Bi_2O_3 and Co_2O_3 co-doping on power loss characteristics of low-temperature-fired NiCuZn ferrites, J. Magn. Magn Mater. 555 (2022).
[23] X.Y. Fan, G.H. Bai, Z.H. Zhang, Q.M. Chen, J.Y. Jin, J.F. Xu, X.F. Zhang, M. Yan, Synergistic effect of V_2O_5 and Bi_2O_3 on the grain boundary structure of high-frequency NiCuZn ferrite ceramics, J. Adv. Ceram. 11 (2022) 912–921.
[24] F. Xie, L.J. Jia, F. Xu, G.W. Gan, J. Li, Y.L. Li, Y.X. Li, H.W. Zhang, Low-temperature sintering LiZnTiMn ferrite ceramics: synthesis, microstructure, and enhanced ferromagnetic properties with CuO-V_2O_5 additive, J. Mater. Sci. Mater. Electron. 29 (2018) 13337–13344.
[25] R.Q. Wang, T.C. Zhou, Z.Y. Zhong, Low-temperature processing of LiZn-based ferrite ceramics by co-doping of V_2O_5 and Sb_2O_3 : composition, microstructure and magnetic properties, J. Mater. Sci. Technol. 99 (2022) 1–8.
[26] Y. Yang, H. Zhang, J. Li, Y. Rao, G. Wang, G. Gan, Bi^{3+} doping-adjusted microstructure, magnetic, and dielectric properties of nickel zinc ferrite ceramics for high frequency LTCC antennas, Ceram. Int. 46 (2020) 25697–25704.
[27] Y.I. Kim, M.K. Jeon, W.B. Im, Crystal structural study of Ho-doped ceria using X-ray powder diffraction data, J. Electroceram. 31 (2013) 254–259.
[28] J.B. Chen, H. Su, Y.L. Jing, Y.X. Li, X.L. Tang, Q.H. Lu, Influence of Cu substitution and Bi_2O_3 doping on magnetic properties of low-temperature-fired NiCuZn ferrites, Ceram. Int. 47 (2021) 20638–20642.
[29] T.C. Zhou, H.W. Zhang, L.J. Jia, Y.L. Liao, Z.Y. Zhong, F.M. Bai, H. Su, J. Li, L. C. Jin, C. Liu, Enhanced ferromagnetic properties of low temperature sintering LiZnTi ferrites with Li_2O-B_2O_3-SiO_2-CaO-Al_2O_3glass addition, J. Alloys Compd. 620 (2015) 421–426.
[30] C. Mallika, O.M. Sreedharan, Thermodynamic stabilities of ternary oxides IN BI-CU-O system by solid-electrolyte EMF method, J. Alloys Compd. 216 (1994) 47–53.
[31] J.H. Jean, C.H. Lee, Processing and properties of low-fire Ni-Cu-Zn ferrite with V_2O_5, JPN. J. Appl. Phys. Part 1-Regular Pape. Short Notes Rev. Pap. 40 (2001) 2232–2236.
[32] F. Gao, J. Li, H.K. Su, Y.H. Sun, Y. Yang, G. Wang, X.N. Han, Q. Li, Low dielectric loss and narrow FMR linewidth of Ca-Ge co-substituted YInIG ferrites for microwave device application, J. Alloys Compd. (2021) 885.
[33] R.C. Pullar, Hexagonal ferrites: a review of the synthesis, properties and applications of hexaferrite ceramics, Prog. Mater. Sci. 57 (2012) 1191–1334.
[34] I. Sharifi, H. Shokrollahi, Nanostructural, magnetic and Mossbauer studies of nanosized $Co_{1-x}Zn_xFe_2O_4$ synthesized by co-precipitation, J. Magn. Magn Mater. 324 (2012) 2397–2403.
[35] G. Aravind, M. Raghasudha, D. Ravinder, Electrical transport properties of nano crystalline Li–Ni ferrites, J. Materiomics 1 (2015) 348–356.
[36] J. Li, B. Lu, Y. Zhang, J. Wu, Y. Yang, X.N. Han, D.D. Wen, Z. Liang, H.W. Zhang, Enhancement of magnetic and dielectric properties of low temperature sintered NiCuZn ferrite by Bi_2O_3-CuO additives, Chin. Phys. B 31 (2022).
[37] L.J. Jia, Y.M. Tang, H.W. Zhang, P.F. Deng, Y.L. Liu, B.Y. Liu, Effects of perovskite additives on the electromagnetic properties of Z-type hexaferrites, Jpn. J. Appl. Phys. 49 (2010).
[38] R.D. Guo, X.F. Zhang, Z. Yu, K. Sun, X.N. Jiang, C.J. Wu, Z.W. Lan, Effects of Bi_2O_3 -$CaCu_3Ti_4O_{12}$ composite additives on micromorphology, static magnetic properties, and FMR linewidth Delta H of NCZ ferrites, Ceram. Int. 46 (2020) 8877–8883.
[39] Q. Li, J. Wang, H.Z. Yao, Soft magnetic, gyromagnetic, and microstructural properties of BBSZ-Nb_2O_5 doped NiCuZn ferrites for LTCC applications, Ceram. Int. 48 (2022) 8653–8660.